

INTEGRATION OF FLUORESCENCE AND REFLECTANCE VISIBLE NEAR-INFRARED (VNIR) HYPERSPECTRAL IMAGES FOR DETECTION OF AFLATOXINS IN CORN KERNELS

F. Zhu, H. Yao, Z. Hruska, R. Kincaid, R. Brown, D. Bhatnagar, T. Cleveland

ABSTRACT. *Aflatoxin contamination in agricultural products has been an important and long-standing problem around the world. Produced by certain fungal species of the Aspergillus genus, aflatoxins are highly toxic and carcinogenic. This study investigated the integration of fluorescence and reflectance visible near-infrared (VNIR) hyperspectral images to detect aflatoxins in whole corn kernels. Field-inoculated corn ears were harvested, and kernels having different aflatoxin contamination levels were collected. Both fluorescence hyperspectral images under ultraviolet (UV) excitation and reflectance hyperspectral images under halogen illumination were recorded on the two sides of the kernels (endosperm and germ). Subsequent chemical analysis was performed on each kernel to provide reference aflatoxin concentration. Threshold values of 20 and 100 ppb were adopted separately to group kernels as contaminated or healthy. Contaminated kernels exhibited different fluorescence and reflectance spectral features compared with healthy kernels. Spectral datasets were compressed and interpreted using principal component analysis (PCA). Least squares support vector machines (LS-SVM) and k-nearest neighbor (KNN) classifiers were used on the fluorescence PC, reflectance PC, and integrated fluorescence and reflectance PC variables for classifying both sides of kernels as contaminated or healthy. The best overall prediction accuracy was 95.33% for the LS-SVM model with the 100 ppb threshold on the germ side in the integrated analysis. Overall, the germ side performed better than the endosperm side, especially for the true positive rate (TPR). Fluorescence and reflectance image data generally achieved similar classification accuracy. The integrated analysis achieved better results than separate fluorescence or reflectance analysis on the germ side, and conspicuous improvement in the TPR of the germ side was observed after integration. The mean aflatoxin concentration in the prediction samples was reduced from 2662.01 ppb to 64.04, 87.33, and 7.59 ppb after removing samples that were classified as contaminated by fluorescence, reflectance, and integrated analysis, respectively, on the germ side. This study demonstrated the potential of the integrated technique for better screening of aflatoxin-contaminated kernels and could lead to rapid and non-destructive scanning-based detection in the corn industry.*

Keywords. *Aflatoxins, Corn kernel, Fluorescence, Hyperspectral imaging, Integration, Reflectance.*

As one of the major agricultural crops around the world, corn has been cultivated for thousands of years (Brown et al., 2013). It is an important source of food and feed, and also provides feedstock for biofuel production (Brown et al., 2013). Contamination by aflatoxins has been an important and chronic problem in the corn industry. Aflatoxins are secondary metabolites produced by aflatoxigenic fungi, primarily *Aspergillus flavus* and *Aspergillus parasiticus*. Aflatoxin contamination is more likely to occur under heat and drought stress in the

field (Payne, 1998) and under improperly managed storage conditions. Because aflatoxins are potent carcinogens associated with severe health hazards in humans and animals (Guo et al., 2008), strict guidelines regarding acceptable limits have been set up in many countries. In the U.S., the action levels for total aflatoxins (B1, B2, G1, G2) are regulated by the U.S. Food and Drug Administration (FDA) and are 20 ppb (parts per billion) for food and 100 ppb for corn and peanut feed products. In the European Union, the limits for aflatoxin B1 and total aflatoxins in food intended for direct human consumption are 2 and 4 ppb, respectively (FAO, 2004). Therefore, it is necessary to eliminate contamination above the regulated levels after harvest and drying in order to prevent aflatoxins from flowing into the food and feed chains. The currently employed methods for aflatoxin analysis, such as high-performance liquid chromatography and thin-layer chromatography, can provide accurate results, but the procedures are usually time-consuming, sample-destructive, and expensive (Turner et al., 2009). Moreover, sampling-based analyses often give a limited view of the contamination level due to the highly uneven distribution of aflatoxins in corn samples (Pearson et al., 2001; Shotwell et al., 1972) and insufficient sampling size.

Submitted for review in May 2015 as manuscript number ITSC 11365; approved for publication by the Information, Technology, Sensors, & Control Systems Community of ASABE in March 2016.

The authors are **Fengle Zhu**, ASABE Member, Postdoctoral Fellow, **Haibo Yao**, ASABE Member, Associate Research Professor, **Zuzana Hruska**, Associate Research Professor, and **Russell Kincaid**, Research Associate, Geosystems Research Institute, Mississippi State University, Stennis Space Center, Mississippi; **Robert Brown**, Research Plant Pathologist, **Deepak Bhatnagar**, Research Leader, and **Thomas Cleveland**, Director, USDA-ARS Southern Regional Research Center, New Orleans, Louisiana. **Corresponding author:** Haibo Yao, 1021 Balch Blvd., Stennis Space Center, MS 39529; phone: 228-688-3742; e-mail: haibo@gri.msstate.edu.

In recent decades, research interest in spectroscopy and hyperspectral imaging techniques has been thriving due to their potential for rapid and non-destructive analysis for food quality and safety with little or no sample preparation. One optical mode commonly adopted for aflatoxin detection in agricultural products is fluorescence under ultraviolet (UV) light excitation. Fluorescence refers to the natural, intrinsic emission of some inorganic or organic substances when excited with high-intensity short-wavelength radiation such as UV lamps or laser sources (Yao et al., 2013b). The emitted fluorescence is usually located in the longer wavelengths and can be captured with spectroscopic measurement or a hyperspectral imaging system. Earlier studies of fluorescence spectra found that aflatoxin-contaminated agricultural products exhibited bright greenish yellow fluorescence (BGYF) under 365 nm UV excitation (Shotwell et al., 1972). BGYF is produced through the reaction of peroxidase in a “living” host plant with kojic acid, which is a secondary metabolite of *A. flavus* (Marsh et al., 1969). The BGYF phenomenon was used as a presumptive test for aflatoxin contamination in corn (Shotwell and Hesseltine, 1981) and various agricultural products (Bothast and Hesseltine, 1975). However, in addition to the subjectivity of BGYF visual inspection and the negative effects of exposure to UV radiation on human health, this method is not reliable. BGYF occurs in healthy corn when infected by non-aflatoxigenic strains (Wicklow, 1999) and may be absent from aflatoxin-contaminated corn with long storage time (FDA, 2014). Fortunately, with the advances in spectroscopic instruments and chemometric algorithms, fluorescence signals of both contaminated and healthy samples were recorded and analyzed to uncover their spectral differences and identify contaminated samples.

Fluorescence spectroscopy and hyperspectral imaging have been applied in the detection of aflatoxin contamination in various agricultural products. Smeesters et al. (2015) investigated the fluorescence spectra of aflatoxin-contaminated and healthy corn samples under different excitation wavelengths. Differences in both of the maximum fluorescence intensity and the emission wavelength were observed for the two groups. The intensity ratio of the integrated fluorescence at 475 to 550 nm to the integrated fluorescence at 400 to 475 nm showed a clear distinction between contaminated and healthy samples. Laser-induced fluorescence spectroscopy was employed to measure the concentration of different types of aflatoxins in pistachio nuts (Paghaleh et al., 2015). Studies using fluorescence hyperspectral imaging under 365 nm UV excitation were carried out to differentiate aflatoxin-contaminated and healthy corn kernels using either mean spectra-based methods (Yao et al., 2010, 2013a) or pixel-based methods (Yao et al., 2013b). The normalized difference fluorescence index (NDFI) with two key wavelengths (437 and 537 nm) was found to have a correlation of 0.81 with aflatoxin concentration in corn kernels (Yao et al., 2013b). For detection of aflatoxin-contaminated and mold-infected figs, fluorescence multispectral imaging was applied, and error rates of 11.98% and 9.38%, respectively, were achieved (Kalkan et al., 2014). The algorithm of local discriminant bases (LDB) was used to extract discriminative features from fluorescence multispectral images for classifi-

cation of aflatoxin-contaminated and healthy hazelnut kernels and red chili peppers, achieving the lowest error rates of 10.34% and 20.83%, respectively (Kalkan et al., 2011).

Another common optical mode is reflectance under halogen light illumination. As Pearson et al. (2001) stated, some chemical and optical properties of whole corn kernels are prone to be affected by prevalent infestation of *Aspergillus* fungi and may be detected with visible near-infrared (VNIR) spectroscopy. Both reflectance (550-1700 nm) and transmittance (500-950 nm) VNIR spectroscopy, in their study, obtained high accuracy in detecting kernels with low (<10 ppb) or high (>100 ppb) aflatoxin levels. Reflectance spectroscopy was also employed for detection of aflatoxin-contaminated corn and barley samples with dispersive (400-2500 nm) and Fourier transform (1112-2500 nm) spectrophotometers (Fernández-Ibañez et al., 2009). Lee et al. (2015) used reflectance near-infrared (NIR) and mid-infrared (MIR) spectroscopy to assess aflatoxin contamination in ground corn samples. Different classification algorithms of linear discriminant analysis (LDA), *k*-nearest neighbor (KNN), and partial least squares discriminant analysis (PLSDA) were applied in the study. The potential of reflectance hyperspectral imaging in the spectral range of 400-1000 nm for early detection of aflatoxigenic fungal strains on corn kernels was described by Del Fiore et al. (2010). Two important wavelengths (410 and 470 nm) were identified, allowing observation of statistical differences in fungal contamination on kernels just 48 h after laboratory inoculation.

In the above investigations concerning aflatoxin detection, a single optical mode was used to acquire either fluorescence or reflectance signals. In a study that classified red chili peppers into aflatoxin-contaminated and healthy groups using hyperspectral imaging, both optical modes were implemented for comparison purposes (Ataş et al., 2012). Because fluorescence and reflectance are different mechanisms by which light interacts with substances, they may be complementary in providing classification information. Both fluorescence and reflectance hyperspectral images were recorded in the present study, which is considered the first attempt to integrate these two kinds of spectra for examining the potential improvement of classification accuracy, while assessing their different contributions to aflatoxin detection in corn kernels.

MATERIALS AND METHODS

SAMPLE PREPARATION

The planting and inoculation of yellow corn plants was carried out in experimental plots at Mississippi State University in Starkville, Mississippi. An aflatoxigenic fungal isolate of *A. flavus* (NRRL 3357) was used to inoculate corn ears at the early dough/late milk stage of kernel development. This fungal strain was obtained from the USDA-ARS Mississippi State University (MSU) research group in Starkville, Mississippi. The isolate was grown in a flask containing 50 g of sterile corncob grits (size 2040, Grit-o-Cobs, Andersons, Inc., Maumee, Ohio) in 100 mL of sterile distilled water. The flask was incubated at 28°C for three

weeks, and the conidia were separated from the grits by rinsing with 500 mL of sterile distilled water containing Tween-20 and subsequent filtering through four layers of sterile cheesecloth. The concentration of conidia was measured using a haemocytometer and adjusted with sterile distilled water to reach a concentration of 9×10^7 conidia mL⁻¹. A 12-gauge stainless steel needle was used to inject about 3.0 mL of inoculum through the husk into kernels for artificial corn ear inoculation. After harvest, the corn ears were shucked, dried, and wiped clean.

Before imaging, all whole corn ears were first examined under UV light to determine the locations of kernels infected with fungi. Three groups of kernels were extracted based on visual inspection. Kernels that showed fluorescence under UV excitation were identified as the glowing group. Kernels that were located directly next to glowing kernels, but did not exhibit fluorescence themselves, were identified as the adjacent group. The control group contained kernels extracted from healthy corn ears or kernels that were far away from the inoculation site. Kernels were carefully extracted from corn ears using a small stainless steel laboratory spatula, and then bagged and labeled. Because the needle inoculation often induced damage to individual kernels, only whole, intact kernels were selected for imaging and further treatments. Altogether, 300 kernels were extracted, with 90, 90, and 120 kernels in the glowing, adjacent, and control groups, respectively.

ACQUISITION OF FLUORESCENCE AND REFLECTANCE HYPERSPECTRAL IMAGES

The hyperspectral imaging system used in this study is shown in figure 1. It is consisted of a 14-bit, high-resolution

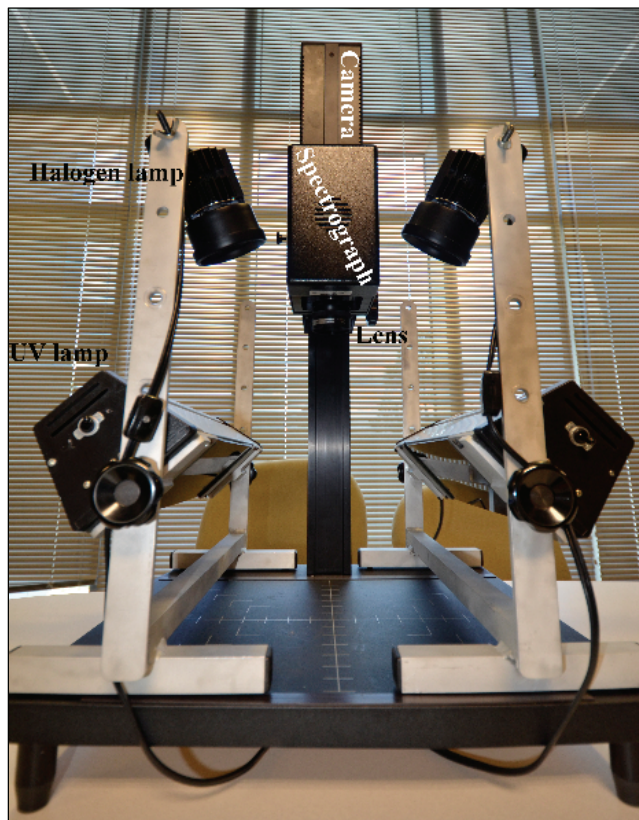


Figure 1. Hyperspectral imaging system.

CCD camera (PCO1600, Cooke Corp., Romulus, Mich.), a spectrograph (ImSpector V10E, Spectral Imaging Ltd., Oulu, Finland), a 35 mm lens, an illumination module, a control computer, a platform, a rigid supporting frame, and an IEEE 1394 Firewire link for transferring image data. The illumination module consisted of two kinds of independent light sources for fluorescence and reflectance measurements. Fluorescence measurement was performed under the excitation of two longwave ultraviolet (UV-A) lamps (model XX-15A, Thermo Fisher Scientific, Waltham, Mass.) with wavelength centered at 365 nm. The excitation filter was mounted in front of the UV lamp to transmit light peaked at 365 nm and block light above 400 nm. In addition, an emission filter was attached in front of the lens to prevent light at wavelengths below approximately 400 nm from entering the spectrograph. For reflectance measurement, two 100 W halogen lamps (Versalite, NRG Research, Inc., Merlin, Ore.) were mounted above targeted samples to provide illumination. The distance from the bottom of the lens to the target was 21.59 cm. More details on the hyperspectral imaging system can be found in Yao et al. (2013b).

Hyperspectral images were acquired in a dark laboratory without external light. For calibrating the fluorescence, a dark current image was recorded after turning off all lights and covering the lens completely with an opaque cap. For calibration of reflectance, in addition to the dark current image, a white reference image was also recorded using a standard white panel (Spectralon SRT-99-100 UV-VIS-NIR diffuse reflectance target, LabSphere, Inc., North Sutton, N.H.). Thirty kernels were arranged in a black-painted, non-reflective, shallow tray that had a grid of small circular depressions to hold individual kernels. Both fluorescence and reflectance measurements were implemented for each tray, with integration times of 500 and 50 ms, respectively. To investigate the spectral difference between the two sides of kernels (endosperm and germ), all kernels were imaged on both sides separately. Thus, 20 fluorescence and 20 reflectance hyperspectral images, including both sides, were recorded in total.

CHEMICAL AFLATOXIN ANALYSIS

After imaging, the kernels were transferred to individually labeled paper bags (one kernel per bag) and placed in a 60°C oven for two days. Each kernel was then subjected to standard chemical analysis for determination of its reference aflatoxin concentration. The chemical procedure for single kernel analysis was adjusted from the AflaTest protocol (VICAM, Milford, Mass.), which is one of the USDA-approved laboratory methods for aflatoxin determination. The detailed procedure for chemical analysis can be found in Yao et al. (2010).

IMAGE PREPROCESSING AND EXTRACTION OF MEAN SPECTRA

The fluorescence and reflectance raw hyperspectral images were preprocessed separately. For fluorescence images, the first preprocessing step was calibration by subtracting the dark current image to remove background sensor noise. The second step was band assignment with appropriate wavelengths. Due to the noisy and weak fluorescence signal

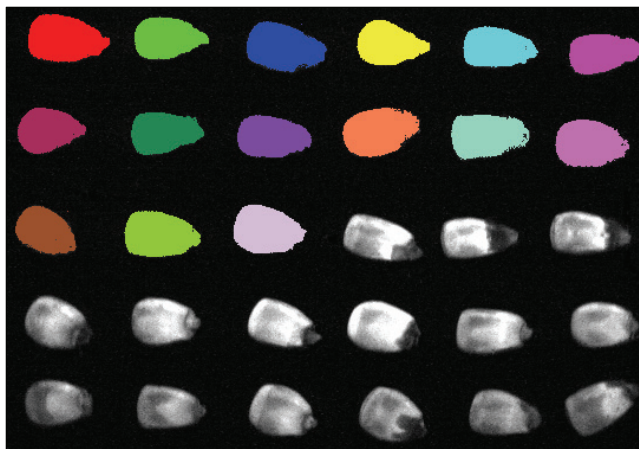


Figure 2. Example of ROI creation through band-thresholding for spectral extraction.

above 700 nm, spectral images with wavelengths ranging from 398.77 to 700.82 nm, with 106 bands, were kept for further processing. The last step was random noise elimination using a low-pass spectral filter (with a window size of five bands) for each pixel. For preprocessing of reflectance images, calibration was carried out as the first step to acquire percentage reflectance based on the dark and white images previously captured. The second step of band assignment and the third step of noise removal were the same as described for fluorescence image preprocessing. The resulting reflectance images had 145 bands with wavelengths from 460.87 to 876.99 nm.

Following preprocessing, hyperspectral images were imported into ENVI software to create a region of interest (ROI) for each kernel through band-thresholding. The adopted threshold values were 50 at band 37 (501.47 nm) for fluorescence images and 15 at band 106 (700.82 nm) for reflectance images. These threshold values were based on an empirical experiment for the best segmenting of kernels and background while keeping the targeted kernel area as large as possible. An example of ROI creation is shown in figure 2. Subsequently, for each ROI, spectra were extracted from all pixels and averaged into one mean spectrum representing the corresponding kernel. This procedure was repeated for all kernel ROIs and implemented with a program in ENVI/IDL (Harris Visual Information Solutions, Boulder, Colo.). For the endosperm and germ sides, two fluorescence spectral matrixes of 300 (number of samples) \times 106 (number of bands) were created, respectively, and two reflectance matrixes of 300 \times 145 were created, respectively.

DATA COMPRESSION AND CLASSIFICATION

The 300 total samples were randomly divided into a training set and a prediction set at a 50/50 ratio. Thus, both sets had 150 samples, with 45, 45, and 60 samples from the glowing, adjacent, and control groups, respectively. For either the fluorescence or reflectance dataset with either the endosperm or germ side, the same training and prediction samples were allocated for comparison and integration purposes. The chosen classification algorithms in the present study were least squares support vector machines (LS-SVM) and *k*-nearest neighbor (KNN). LS-SVM (proposed by Suykens et

al., 2002) are reformulations of standard SVM that lead to solving linear equations instead of a quadratic programming problem. Thus, nonlinear multivariate classification and regression problems can be solved using LS-SVM with lower computational cost. KNN is another classical machine learning method, and it is very simple and intuitive. It classifies unlabeled examples based on their similarity with examples in the training set. In this study, the extracted spectral data, with more than 100 variables, were usually intercorrelated and even redundant, and more variables would be introduced if fluorescence and reflectance data were integrated in raw format. Because KNN calculates the Euclidean distances from the newly fed prediction sample to all training samples along all dimensions, spectral dimension reduction prior to classification was necessary and might improve the classification efficiency and accuracy.

Principal component analysis (PCA), a widely used method for data compression and interpretation as well as information extraction, was adopted. Through orthogonal transformation, PCA finds far fewer independent components to maximize representation of the original data. Thus, redundant data can be largely reduced without losing much useful information. In the present study, fluorescence and reflectance spectral information from one side of the kernels (endosperm or germ) was integrated after their separate PCA compression. However, the data range of fluorescence and reflectance spectra are quite different due to the different calibration procedures for fluorescence and reflectance images. Therefore, it is indispensable to normalize each dataset individually prior to PCA. Moreover, to maintain independence between the training and prediction datasets, regardless of the dataset analyzed (fluorescence with endosperm or germ, and reflectance with endosperm or germ), data normalization and PCA calculation were not carried out at one time for the total data of 300 samples. Instead, first only the spectral variables of the training dataset were normalized and rotated to PC spaces, and then the spectral variables of the prediction dataset were normalized, using the same transforming rule used by the training dataset, and then projected to the same PC spaces as the rotated training dataset. MATLAB (MathWorks, Natick, Mass.) was used for PCA analysis.

After PCA calculation, based on the percentage of the total variance explained by each PC in the training samples, a few first PC variables were retained from both the training and prediction sets to substitute for the original spectral variables. According to FDA regulations regarding aflatoxin action levels in food and corn feed, two thresholds (20 and 100 ppb) were used separately to label each kernel sample as contaminated (+1) or healthy (-1). Hence, for each dataset analysis (fluorescence or reflectance or combined fluorescence and reflectance) with endosperm or germ side, two kinds of classification problems with different threshold values had to be addressed. Of the 300 kernels individually analyzed for aflatoxins, 79 contained aflatoxin levels greater than or equal to 20 ppb, 75 contained aflatoxin levels greater than or equal to 100 ppb, 59 contained aflatoxin levels greater than or equal to 2000 ppb, and 26 contained aflatoxin levels greater than or equal to 10,000 ppb. Based on the 20 ppb threshold, 79 samples (41 for training, 38 for prediction) were labeled as contaminated, while the remaining 221

(109 for training, 112 for prediction) were healthy. Based on the 100 ppb threshold, there were 75 (38 for training, 37 for prediction) contaminated samples and 225 (112 for training, 113 for prediction) healthy samples.

The compressed PC variables and their corresponding Y values (-1 or +1) were then imported into the LS-SVM and KNN algorithms, respectively, to classify samples as contaminated or healthy. The LS-SVM classifier with radial basis function (RBF) kernel was implemented in MATLAB. For the KNN classifier, a cross-validation method was employed to determine the best k value, with the maximum value for k set as 11 in Weka software (Hall et al., 2009). Additionally, because the number of healthy samples was higher than that of contaminated samples in this study, distance weighting with $1/\text{distance}$ was used in KNN to balance the problem of uneven distribution of the samples.

RESULTS AND DISCUSSION

OVERVIEW OF FLUORESCENCE AND REFLECTANCE SPECTRAL CURVES

The mean fluorescence spectra of kernels (endosperm and germ sides) are shown in figure 3a for the three visually designated groups (glowing, adjacent, and control) and in figure 3b for the three contamination groups (above 100 ppb, 20 to 100 ppb, and below 20 ppb). The corn fluorescence

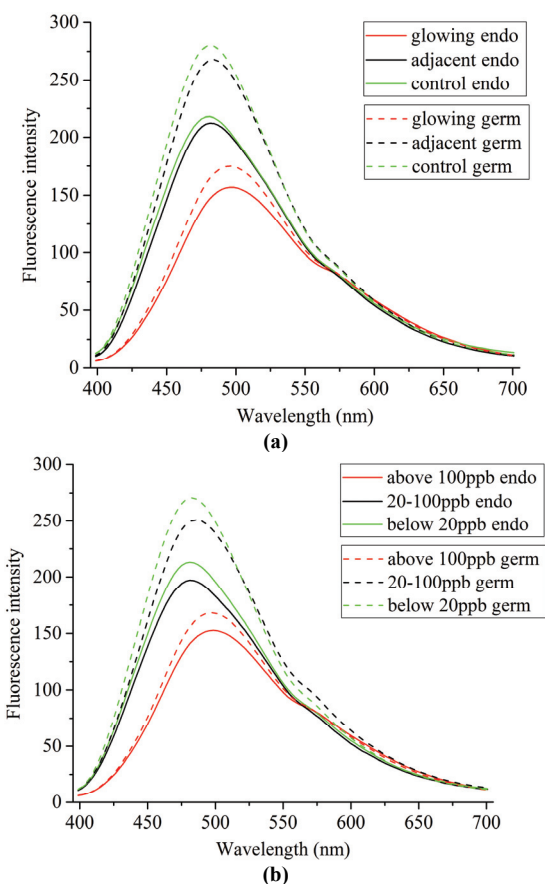


Figure 3. Mean fluorescence spectral curves for (a) three visually designated groups (glowing, adjacent, and control) and (b) three contamination groups (above 100 ppb, 20 to 100 ppb, and below 20 ppb) with both endosperm and germ sides.

emission signal is mainly distributed in the blue and green regions, with an emission peak located in the range of 450 to 500 nm.

In figure 3a, the spectral curves are very similar for the endosperm and germ sides, except for the higher fluorescence intensity exhibited by the germ side. A fluorescence peak shift was observed among the three groups of kernels. Peaks of control groups are located at shorter wavelengths, while peaks of glowing groups are obviously shifted toward longer wavelengths. Another difference among the three groups is the fluorescence intensity, with both glowing groups exhibiting the lowest fluorescence signals. For the glowing kernels, the glow identifiable by human eyes under UV excitation is referred to as BGYP. As discussed earlier, BGYP visual inspection is no longer regarded as a reliable indication of aflatoxin contamination. However, in this study where corn was artificially inoculated with an aflatoxigenic strain of *A. flavus*, glowing kernels generally had very high contamination levels.

For the above reason, the fluorescence spectral curves of the glowing groups in figure 3a were similar to those of groups with aflatoxin above 100 ppb in figure 3b, where the latter groups had peaks shifted slightly to longer wavelengths. The differences in both the peak shift and fluorescence intensity between the glowing groups and the other groups in figure 3a were also observed in figure 3b for the different contamination groups. In particular, kernels with higher contamination levels had fluorescence peaks shifted to longer wavelengths with lower intensity. The peak shifts from the groups with aflatoxin below 20 ppb to the groups with aflatoxin above 100 ppb were around 17 nm for both the endosperm and germ sides. This observation might provide important clues for aflatoxin detection. Similar spectral changes in corn kernels caused by aflatoxin contamination were reported in previous studies (Smeesters et al., 2015; Yao et al., 2010, 2013a, 2013b). The peak shift from contaminated corn kernels might be induced by the production of secondary metabolites, such as kojic acid and aflatoxins, by *A. flavus* (Klich, 2007). Because the group with aflatoxin levels between 20 and 100 ppb in this study contained only four samples, the small sample size might not provide representative spectral curves for the 20 to 100 ppb group, especially on the endosperm side. This is the reason for the absence of a fluorescence peak difference between the 20 to 100 ppb group and the <20 ppb group for the endosperm side. However, a peak difference of about 6 nm was observed for the germ side. This might indicate higher fluorescence sensitivity of the germ side to aflatoxin contamination, and thus the germ side might be more useful in differentiating contaminated and healthy kernels using fluorescence spectra.

Figure 4 shows the mean reflectance spectra for the three visually designated groups (fig. 4a) and the three contamination groups (fig. 4b) for both sides of the kernels. No obvious differences existed between the endosperm and germ sides for all groups in terms of curve shape and reflectance magnitude. As explained before, the reflectance spectral curves of the glowing groups in figure 4a tended to be similar to those of the groups with aflatoxin above 100 ppb in figure 4b. In comparison with the other groups, these two

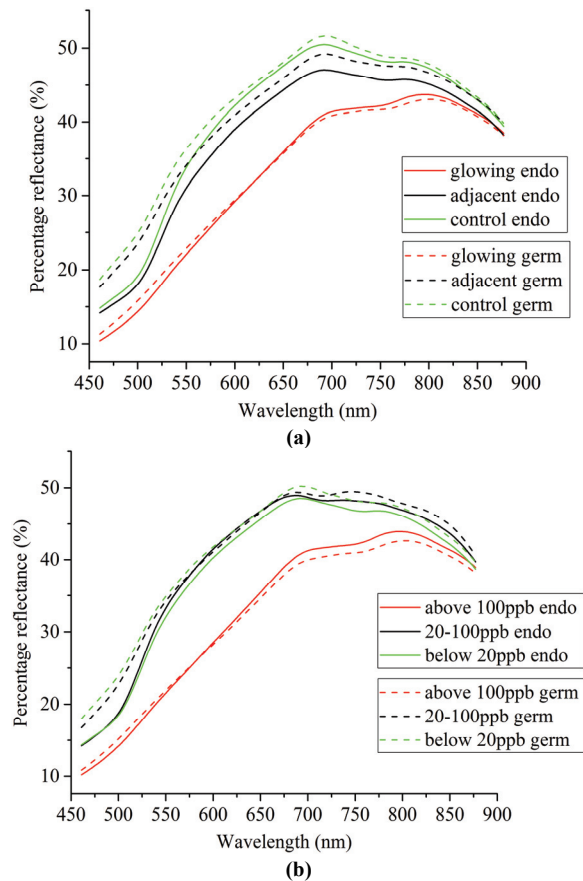


Figure 4. Mean reflectance spectral curves for (a) three visually designated groups (glowing, adjacent, and control) and (b) three contamination groups (above 100 ppb, 20 to 100 ppb, and below 20 ppb) with both endosperm and germ sides.

groups (glowing groups and ≥ 100 ppb groups) had distinct features. One aspect was their lower percentage reflectance. This was similar to the phenomenon of higher absorbance (lower reflectance, as absorbance = $\log[1/\text{reflectance}]$) below 850 nm for kernels with aflatoxin greater than 100 ppb, as reported by Pearson et al. (2001). The discoloration of the contaminated kernels might be the primary reason for the lower reflectance values (Pearson et al., 2001). Another aspect was the different shape of their reflectance curves compared with those of the other groups. The main difference occurred in the range of approximately 700 to 800 nm, where the reflectance of the glowing groups and the ≥ 100 ppb groups increased, while reflectance of all other groups decreased in that range. This might provide important information for classifying contaminated and healthy kernels. In figure 4b, for both endosperm and germ sides, the reflectance magnitudes of the 20 to 100 ppb groups and the < 20 ppb groups were similar, which might be due to the small sample size for aflatoxin levels between 20 and 100 ppb. However, compared with the < 20 ppb groups, the reflectance of 20 to 100 ppb groups decreased more slowly from 700 to 800 nm, which might be a sign of intermediate aflatoxin contamination.

PCA INTERPRETATION

Overall, four spectral datasets (fluorescence with endosperm or germ, and reflectance with endosperm or germ) were compressed and interpreted separately using PCA. Regardless of which dataset was analyzed, PCA calculations on the training samples showed that the first three PC scores could explain over 99% of the total data variance. Thus, the first three PCs were good representations of the original spectral information and were retained for both the training and prediction sets. Figure 5 shows scatter plots of the first three PC variables of the training samples for fluorescence and reflectance spectra with both endosperm and germ sides. Sample points are marked as contaminated or healthy with the 20 ppb threshold. Although PCA calculation is only based on the spectral information of kernels without considering their labeled classes, a certain degree of separation of the contaminated and healthy groups was observed in all four plots, which demonstrates the spectral changes in corn kernels caused by aflatoxin contamination. The separability was similar using either fluorescence or reflectance with either the endosperm or germ side. In comparison with healthy samples, contaminated samples generally showed a larger variance due to their variable aflatoxin concentrations. Slightly better separation might be presented using the 100 ppb threshold (data not shown). However, the PC scatter plots only give visual separation of contaminated and healthy samples. Classification algorithms were then applied to the PC variables in both the training and prediction sets to provide accurate separation results.

CLASSIFICATION OF CONTAMINATED AND HEALTHY KERNELS

After PCA calculation, four sets of PC variables (fluorescence with endosperm or germ, and reflectance with endosperm or germ) were extracted. For integrating different optical techniques, fluorescence and reflectance PC variables from one side of the kernels (endosperm or germ) were combined. Thus, six sets of PC variables were used to classify contaminated and healthy samples based on the thresholds of 20 and 100 ppb. The LS-SVM and KNN classification results (confusion matrix) of the prediction samples for both sides of the kernels using fluorescence, reflectance, and integrated fluorescence and reflectance are shown in tables 1, 2, and 3, respectively.

In these three tables, all models achieved satisfactory accuracy for classifying contaminated and healthy kernels. The best overall accuracy was 95.33% for the LS-SVM model with the 100 ppb threshold on the germ side in the integrated analysis (table 3). Overall, KNN achieved classification results comparable with those of LS-SVM, although it is a much simpler algorithm. The advantage of LS-SVM was more obvious only in the reflectance analysis. The results based on the 100 ppb threshold were in general slightly superior to the results based on the 20 ppb threshold. This may have occurred because of greater similarity between samples with aflatoxin levels between 20 and 100 ppb and with < 20 ppb than with the ≥ 100 ppb samples in both the fluorescence and reflectance spectra.

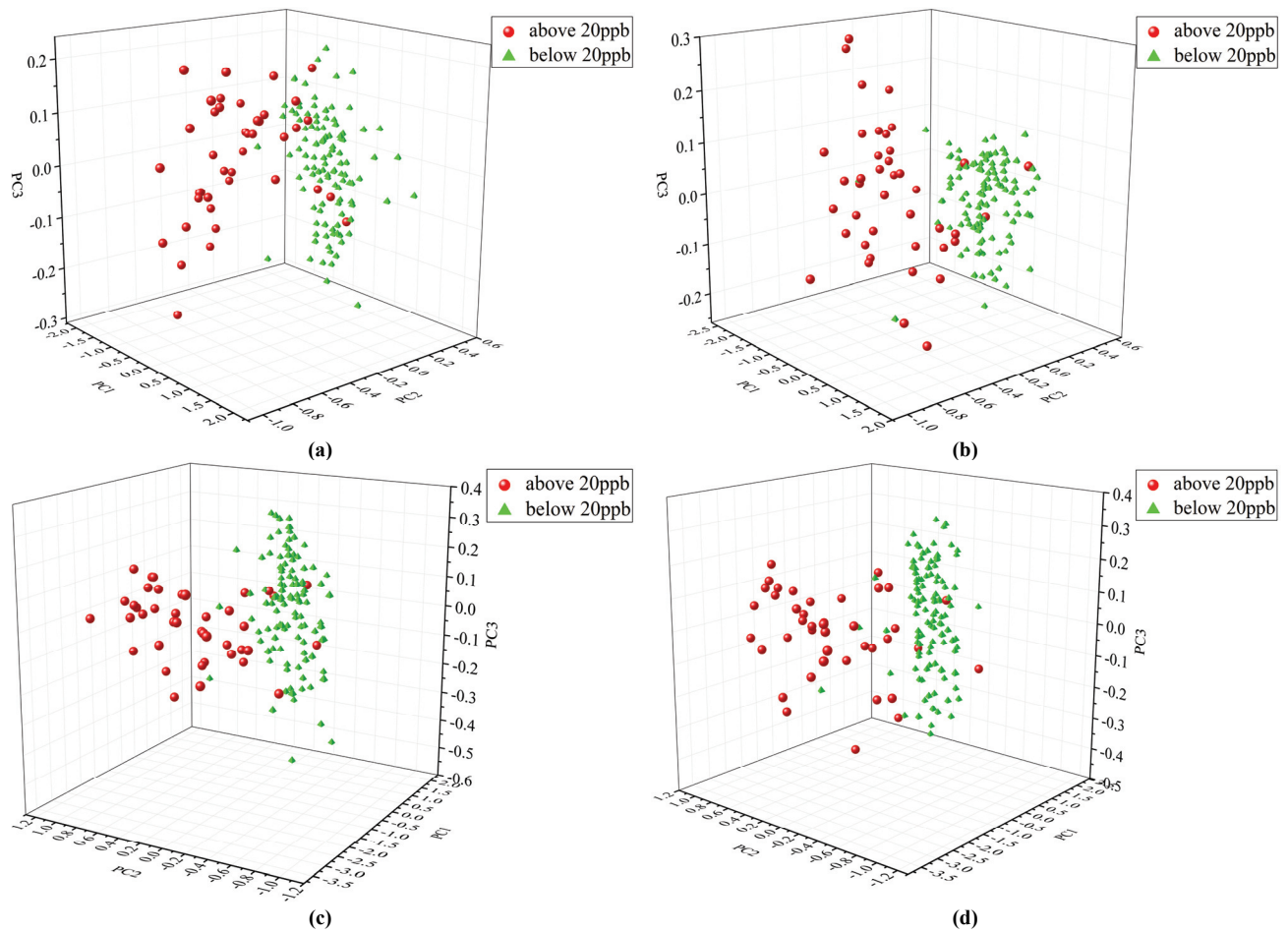


Figure 5. Scatter plots of the first three PC variables of training samples for fluorescence spectra with (a) endosperm and (b) germ sides and reflectance spectra with (c) endosperm and (d) germ sides.

Table 1. Classification results for prediction samples on both sides of corn kernels using fluorescence spectra.

Sample Group (and Threshold)		LS-SVM			KNN		
		Classified as Contaminated (%)	Classified as Healthy (%)	Overall Accuracy (%)	Classified as Contaminated (%)	Classified as Healthy (%)	Overall Accuracy (%)
Endosperm (20 ppb)	Contaminated	73.68	26.32	90.00	73.68	26.32	86.67
	Healthy	4.46	95.54		8.93	91.07	
Endosperm (100 ppb)	Contaminated	75.68	24.32	90.67	75.68	24.32	91.33
	Healthy	4.42	95.58		3.54	96.46	
Germ (20 ppb)	Contaminated	81.58	18.42	92.67	84.21	15.79	92.67
	Healthy	3.57	96.43		4.46	95.54	
Germ (100 ppb)	Contaminated	83.78	16.22	93.33	86.49	13.51	93.33
	Healthy	3.54	96.46		4.42	95.58	

Table 2. Classification results for prediction samples on both sides of corn kernels using reflectance spectra.

Sample Group (and Threshold)		LS-SVM			KNN		
		Classified as Contaminated (%)	Classified as Healthy (%)	Overall Accuracy (%)	Classified as Contaminated (%)	Classified as Healthy (%)	Overall Accuracy (%)
Endosperm (20 ppb)	Contaminated	78.95	21.05	92.67	76.32	23.68	90.00
	Healthy	2.68	97.32		5.36	94.64	
Endosperm (100 ppb)	Contaminated	83.78	16.22	94.00	75.68	24.32	90.00
	Healthy	2.65	97.35		5.31	94.69	
Germ (20 ppb)	Contaminated	84.21	15.79	92.67	81.58	18.42	90.67
	Healthy	4.46	95.54		6.25	93.75	
Germ (100 ppb)	Contaminated	86.49	13.51	94.00	81.08	18.92	90.67
	Healthy	3.54	96.46		6.19	93.81	

Table 3. Classification results for prediction samples on both sides of corn kernels using combined fluorescence and reflectance spectra.

Sample Group (and Threshold)		LS-SVM			KNN		
		Classified as Contaminated (%)	Classified as Healthy (%)	Overall Accuracy (%)	Classified as Contaminated (%)	Classified as Healthy (%)	Overall Accuracy (%)
Endosperm (20 ppb)	Contaminated	76.32	23.68	90.00	78.95	21.05	92.00
	Healthy	5.36	94.64		3.57	96.43	
Endosperm (100 ppb)	Contaminated	83.78	16.22	93.33	78.38	21.62	91.33
	Healthy	3.54	96.46		4.42	95.58	
Germ (20 ppb)	Contaminated	89.47	10.53	94.67	89.47	10.53	94.67
	Healthy	3.57	96.43		3.57	96.43	
Germ (100 ppb)	Contaminated	91.89	8.11	95.33	89.19	10.81	94.00
	Healthy	3.54	96.46		4.42	95.58	

Except for the LS-SVM prediction results in the reflectance analysis, the classification results for the germ side were better than those for the endosperm side. Additionally, the accuracy of contaminated samples classified as contaminated (true positive rate, TPR) was higher for the germ side than for the endosperm side for all classification models. Compared with the endosperm side, the averaged TPR of the germ side was 9.33%, 4.66%, 10.65% higher using fluorescence, reflectance, and integrated fluorescence and reflectance, respectively. TPR is particularly important if the primary concern of classification is discarding contaminated kernels to avoid aflatoxin entering the food and feed markets. In a study using reflectance VNIR spectroscopy for aflatoxin detection in corn kernels (Pearson et al., 2001), spectra collected from the germ side also performed better. A possible explanation could be that after injecting inoculum into the corn ear, fungal infection progressed from the inside of the ear through the tip cap and into the oil-rich germ side first (Gao and Kolomiets, 2009; Pearson and Wicklow, 2006) and thus would be more prevalent in the germ (Pearson et al., 2001). Because the germ side was more useful in discriminating contaminated and healthy kernels, for either single or integrated measurements, a screening system capable of determining kernel orientation might improve detection accuracy, especially for higher TPR.

Although fluorescence and reflectance have different optical mechanisms in interacting with substances, they generally achieved similar classification accuracies, except that the results for the endosperm and germ sides in the reflectance analysis were closer than those in the fluorescence analysis. Compared with reflectance, fluorescence intensity was relatively lower, even with prolonged data acquisition time, due to the low fluorescence quantum yields from biological samples under UV-A light excitation (Zhang et al., 2012). A more powerful UV excitation source might be helpful in generating stronger fluorescence emissions. A more efficient CCD light quantum catching camera could also potentially accelerate data acquisition and improve detection accuracy for fluorescence hyperspectral imaging. Reflectance mode is easier to operate than fluorescence mode and has proven to be a valuable tool in classifying contaminated and healthy kernels in this study. However, most of the reflectance VNIR light reaching the sensor may have interacted only with the kernel surface, revealing mainly the color alteration induced by aflatoxin contamination. Because discoloration of kernels could also occur when corn ears are infected with other types of fungi (Pearson and Wicklow, 2006) or even insects, aflatoxin detection accuracy based on

reflectance spectra might diminish in situations where cross-contamination occurs. In contrast, fluorescence is considered a sensitive optical technique for detecting subtle changes in biological materials (Kim et al., 2003). Therefore, fluorescence and reflectance may complement each other in providing classification information.

The integration of fluorescence and reflectance spectra achieved better classification results than separate fluorescence or reflectance analysis only for the germ side and was 2.00% and 1.34% higher in average for the 20 and 100 ppb based classifications, respectively, than using fluorescence alone, and 3.00% and 2.33% higher in average for the 20 and 100 ppb based classifications, respectively, than using reflectance alone. Although the overall improvement in accuracy is not impressive, the TPR of the germ side increased from an average of 84.02% in the fluorescence analysis and 83.34% in the reflectance analysis to an average of 90.01% in the integrated analysis. The mean aflatoxin concentration in the prediction samples was 2662.01 ppb prior to classification. This high value was derived from the generally high aflatoxin level of contaminated kernels in this study in spite of the lower number of contaminated kernels compared to healthy kernels. The mean aflatoxin concentration was also calculated separately after removal of samples that were classified as contaminated by all models for the germ side. The calculated values were pooled for the different models with different thresholds for fluorescence analysis, reflectance analysis, and integrated analysis, showing that the mean aflatoxin concentration decreased to 64.04, 87.33, and 7.59 ppb, respectively. Therefore, the integration technique for the germ side has potential for accurate and thorough elimination of contaminated kernels.

This study was designed as a laboratory-based exploratory investigation using artificially field-inoculated corn. To detect naturally occurring aflatoxins in corn kernels in grain elevators or critical processing points, multiple stages of work are needed to extrapolate the findings of this work into a practical application. For example, the distribution of contaminated and healthy samples was uneven and skewed in the present study. Kernels were either heavily contaminated or clean, and the number of intermediately contaminated kernels was low. This is because the kernels were collected from fully ripened corn ears with moisture contents lower than 15% two months after artificial inoculation in the field. Larger amounts of intermediately contaminated kernels will be collected in future experiments by harvesting corn ears at different time intervals after field inoculation. In addition, full wavelength ranges of both fluorescence and reflectance

were used in this study to fully explore the potential of spectral integration. Considering the two key wavelengths (437 and 537 nm) for fluorescence measurement identified by Yao et al. (2013b), identification of a few key wavelengths for reflectance measurement should be carried out to further study the integration of fluorescence and reflectance for faster detection. Furthermore, although the yellow corn used in this study is the most common variety, other corn varieties have various colors, which could affect the visible reflectance spectra. Different varieties of corn kernels should be tested in future experiments.

CONCLUSIONS

For the classification of aflatoxin-contaminated and healthy corn kernels, both fluorescence and reflectance VNIR hyperspectral images were employed for integration and comparison purposes. In comparison with healthy kernels, the fluorescence spectral curves of contaminated kernels had peaks shifted to longer wavelengths with lower intensity, and the reflectance values of contaminated kernels were generally lower with a different trend in the range of 700 to 800 nm. The first three PC variables of the training samples showed a certain degree of visual separation for contaminated and healthy sample groups using either fluorescence or reflectance spectra with the endosperm or germ side. LS-SVM and KNN classifiers were used on the fluorescence PC, reflectance PC, and integrated fluorescence and reflectance PC variables on both the endosperm and germ sides. The best overall prediction accuracy of 95.33% was achieved by the LS-SVM model for the 100 ppb threshold on the germ side in the integrated analysis. Overall, the classification results were better for the germ side than for the endosperm side, especially for TPR.

Fluorescence and reflectance image data generally achieved similar classification results, although they have different optical mechanisms. Reflectance is stronger than fluorescence, with easier acquisition, but it is not as sensitive and intrinsic as fluorescence. The integrated analysis achieved better results than separate fluorescence or reflectance analysis on the germ side. Conspicuous improvement in TPR was observed on the germ side, increasing from an average of 84.02% in the fluorescence analysis and 83.34% in the reflectance analysis to an average of 90.01% in the integrated analysis. Additionally, the mean aflatoxin concentration in the prediction samples decreased from 2662.01 ppb to 64.04, 87.33, and 7.59 ppb after the removal of samples that were classified as contaminated when using fluorescence, reflectance, and integrated analysis, respectively, on the germ side. The results so far have demonstrated the potential of the proposed integration technique for more accurate detection of aflatoxins in corn kernels. As fluorescence and reflectance measurements can be made with the same imaging system, further endeavors in the collection of larger numbers of kernels with intermediate contamination levels, identification of a few key wavelengths for reflectance measurement, and testing of different varieties of corn kernels might lead to rapid and non-destructive detection of carcinogenic aflatoxins in the corn industry.

ACKNOWLEDGEMENTS

Funding for this work was provided by the USDA (Cooperative Agreement No. 58-6435-3-121) and the U.S. Agency for International Development via the Peanut Mycotoxin Innovation Laboratory at University of Georgia (Subaward No. RC710-059/4942206). The authors would like to thank Drs. Gary Windham and William Paul Williams of the USDA-ARS in Mississippi State, Mississippi, for help with producing the corn samples for this study and providing the inoculum.

REFERENCES

- Ataş, M., Yardimci, Y., & Temizel, A. (2012). A new approach to aflatoxin detection in chili pepper by machine vision. *Comput. Electron. Agric.*, 87, 129-141. <http://dx.doi.org/10.1016/j.compag.2012.06.001>
- Bothast, R. J., & Hesseltine, C. W. (1975). Bright greenish-yellow fluorescence and aflatoxin in agricultural commodities. *Appl. Environ. Microbiol.*, 30(2), 337-338.
- Brown, R. L., Menkir, A., Chen, Z. Y., Bhatnagar, D., Yu, J., Yao, H., & Cleveland, T. E. (2013). Breeding aflatoxin-resistant maize lines using recent advances in technologies: A review. *Food Addit. Contam. A*, 30(8), 1382-1391. <http://dx.doi.org/10.1080/19440049.2013.812808>
- Del Fiore, A., Reverberi, M., Ricelli, A., Pinzari, F., Serranti, S., Fabbri, A. A., ... Fanelli, C. (2010). Early detection of toxigenic fungi on maize by hyperspectral imaging analysis. *Intl. J. Food Microbiol.*, 144(1), 64-71. <http://dx.doi.org/10.1016/j.ijfoodmicro.2010.08.001>
- FAO. (2004). Worldwide regulations for mycotoxins in food and feed in 2003. FAO Food and Nutrition Paper 81. Rome, Italy: United Nations FAO.
- FDA. (2014). Chapter 4: Sampling. In *Investigations Operations Manual 2014* (pp. 108-213). Washington, D.C.: FDA.
- Fernández-Ibañez, V., Soldado, A., Martínez-Fernández, A., & de la Roza-Delgado, B. (2009). Application of near-infrared spectroscopy for rapid detection of aflatoxin B1 in maize and barley as analytical quality assessment. *Food Chem.*, 113(2), 629-634. <http://dx.doi.org/10.1016/j.foodchem.2008.07.049>
- Gao, X., & Kolomiets, M. V. (2009). Host-derived lipids and oxylipins are crucial signals in modulating mycotoxin production by fungi. *Toxin Reviews*, 28(2-3), 79-88. <http://dx.doi.org/10.1080/15569540802420584>
- Guo, B., Chen, Z. Y., Lee, R. D., & Scully, B. T. (2008). Drought stress and preharvest aflatoxin contamination in agricultural commodity: Genetics, genomics, and proteomics. *J. Integr. Plant Biol.*, 50(10), 1281-1291. <http://dx.doi.org/10.1111/j.1744-7909.2008.00739.x>
- Hall, M., Frank, E., Holmes, G., Pfahringer, B., Reutemann, P., & Witten, I. H. (2009). The WEKA data mining software: An update. *ACM SIGKDD Explorations Newsletter*, 11(1), 10-18. <http://dx.doi.org/10.1145/1656274.1656278>
- Kalkan, H., Beriat, P., Yardimci, Y., & Pearson, T. C. (2011). Detection of contaminated hazelnuts and ground red chili pepper flakes by multispectral imaging. *Comput. Electron. Agric.*, 77(1), 28-34. <http://dx.doi.org/10.1016/j.compag.2011.03.005>
- Kalkan, H., Güneş, A., Durmuş, E., & Kuşçu, A. (2014). Non-invasive detection of aflatoxin-contaminated figs using fluorescence and multispectral imaging. *Food Addit. Contam. A*, 31(8), 1414-1421. <http://dx.doi.org/10.1080/19440049.2014.926398>
- Kim, M. S., Lefcourt, A. M., & Chen, Y. R. (2003). Multispectral laser-induced fluorescence imaging system for large biological

- samples. *Appl. Opt.*, 42(19), 3927-3934.
<http://dx.doi.org/10.1364/AO.42.003927>
- Klich, M. A. (2007). *Aspergillus flavus*: The major producer of aflatoxin. *Molec. Plant Pathol.*, 8(6), 713-722.
<http://dx.doi.org/10.1111/j.1364-3703.2007.00436.x>
- Lee, K. M., Davis, J., Herrman, T. J., Murray, S. C., & Deng, Y. (2015). An empirical evaluation of three vibrational spectroscopic methods for detection of aflatoxins in maize. *Food Chem.*, 173, 629-639.
<http://dx.doi.org/10.1016/j.foodchem.2014.10.099>
- Marsh, P. B., Simpson, M. E., Ferretti, R. J., Merola, G. V., Donoso, J., Craig, G. O., ... Work, P. S. (1969). Mechanism of formation of a fluorescence in cotton fiber associated with aflatoxins in the seeds at harvest. *J. Agric. Food. Chem.*, 17(3), 468-472. <http://dx.doi.org/10.1021/jf60163a006>
- Paghaleh, S. J., Askari, H. R., Marashi, S. M. B., Rahimi, M., & Bahrapour, A. R. (2015). A method for the measurement of in line pistachio aflatoxin concentration based on the laser induced fluorescence spectroscopy. *J. Lumin.*, 161, 135-141.
<http://dx.doi.org/10.1016/j.jlumin.2014.12.057>
- Payne, G. A. (1998). Process of contamination by aflatoxin-producing fungi and their impact on crops. In (K. K. Sinha & D. Bhatnagar, Eds.), *Mycotoxins in Agriculture and Food Safety* (pp. 279-306) New York, N.Y.: Marcel Dekker.
- Pearson, T. C., & Wicklow, D. T. (2006). Detection of corn kernels infected by fungi. *Trans. ASABE*, 49(4), 1235-1245.
<http://dx.doi.org/10.13031/2013.21723>
- Pearson, T. C., Wicklow, D. T., Maghirang, E. B., Xie, F., & Dowell, F. E. (2001). Detecting aflatoxin in single corn kernels by transmittance and reflectance spectroscopy. *Trans. ASAE*, 44(5), 1247-1254. <http://dx.doi.org/10.13031/2013.6418>
- Shotwell, O. L., & Hesseltine, C. W. (1981). Use of bright greenish yellow fluorescence as a presumptive test for aflatoxin in corn. *Cereal Chem.*, 58(2), 124-127.
- Shotwell, O. L., Goulden, M. L., & Hesseltine, C. W. (1972). Aflatoxin contamination: Association with foreign material and characteristic fluorescence in damaged corn kernels. *Cereal Chem.*, 49, 458-465.
- Smeesters, L., Meulebroeck, W., Raeymaekers, S., & Thienpont, H. (2015). Optical detection of aflatoxins in maize using one- and two-photon induced fluorescence spectroscopy. *Food Control*, 51, 408-416. <http://dx.doi.org/10.1016/j.foodcont.2014.12.003>
- Suykens, J. A., Van Gestel, T., De Brabanter, J., & De Moor, B. V. (2002). *Least Squares Support Vector Machines*. Singapore: World Scientific.
- Turner, N. W., Subrahmanyam, S., & Piletsky, S. A. (2009). Analytical methods for determination of mycotoxins: A review. *Anal. Chim. Acta*, 632(2), 168-180.
<http://dx.doi.org/10.1016/j.aca.2008.11.010>
- Wicklow, D. T. (1999). Influence of *Aspergillus flavus* strains on aflatoxin and bright greenish yellow fluorescence of corn kernels. *Plant Disease*, 83(12), 1146-1148.
<http://dx.doi.org/10.1094/PDIS.1999.83.12.1146>
- Yao, H., Hruska, Z., Kincaid, R., Brown, R. L., Bhatnagar, D., & Cleveland, T. E. (2013a). Detecting maize inoculated with toxigenic and atoxigenic fungal strains with fluorescence hyperspectral imagery. *Biosystems Eng.*, 115(2), 125-135.
<http://dx.doi.org/10.1016/j.biosystemseng.2013.03.006>
- Yao, H., Hruska, Z., Kincaid, R., Brown, R. L., Bhatnagar, D., & Cleveland, T. E. (2013b). Hyperspectral image classification and development of fluorescence index for single corn kernels infected with *Aspergillus flavus*. *Trans. ASABE*, 56(5), 1977-1988. <http://dx.doi.org/10.13031/trans.56.10091>
- Yao, H., Hruska, Z., Kincaid, R., Brown, R. L., Cleveland, T. E., & Bhatnagar, D. (2010). Correlation and classification of single kernel fluorescence hyperspectral data with aflatoxin concentration in corn kernels inoculated with *Aspergillus flavus* spores. *Food Addit. Contam. A*, 27(5), 701-709.
<http://dx.doi.org/10.1080/19440040903527368>
- Zhang, R., Ying, Y., Rao, X., & Li, J. (2012). Quality and safety assessment of food and agricultural products by hyperspectral fluorescence imaging. *J. Sci. Food Agric.*, 92(12), 2397-2408.
<http://dx.doi.org/10.1002/jsfa.5702>